

Fast, Modular, and Differentiable Framework for Machine Learning-Enhanced Molecular Simulations

Henrik Christiansen,* Takashi Maruyama, Federico Errica,
Viktor Zaverkin, Makoto Takamoto, and Francesco Alesiani
NEC Laboratories Europe GmbH, Kurfürsten-Anlage 36, 69115 Heidelberg, Germany
(Dated: March 27, 2025)

We present an end-to-end differentiable molecular simulation framework (DIMOS) for molecular dynamics and Monte Carlo simulations. DIMOS easily integrates machine-learning-based interatomic potentials and implements classical force fields including particle-mesh Ewald electrostatics. Thanks to its modularity, both classical and machine-learning-based approaches can be easily combined into a hybrid description of the system (ML/MM). By supporting key molecular dynamics features such as efficient neighborlists and constraint algorithms for larger time steps, the framework bridges the gap between hand-optimized simulation engines and the flexibility of a PyTorch implementation. The superior performance and the high versatility is probed in different benchmarks and applications, with speed-up factors of up to $170\times$. The advantage of differentiability is demonstrated by an end-to-end optimization of the proposal distribution in a Markov Chain Monte Carlo simulation based on Hamiltonian Monte Carlo. Using these optimized simulation parameters a $3\times$ acceleration is observed in comparison to ad-hoc chosen simulation parameters. The code is available at <https://github.com/nec-research/DIMOS>.

Molecular simulations are a cornerstone of modern computational physics, chemistry and biology, enabling researchers to understand complex properties of the system [1]. Traditional molecular dynamics (MD) and Markov Chain Monte Carlo (MCMC) simulations rely on pre-defined force fields and specialized software to achieve large timescales and efficient sampling of rugged free-energy landscapes [2]. However, conventional MD and MCMC simulation packages generally lack the flexibility and modularity to easily incorporate cutting-edge computational techniques such as machine learning (ML) based enhancements: Advances in machine learning interatomic potentials (MLIPs) promise improved accuracy for MD simulations [3], yet integrating these techniques into a scalable and user-friendly framework remains a major challenge, especially when developing novel approaches [4].

Here we present an end-to-end differentiable molecular simulation framework (DIMOS) implemented in PyTorch [5], a popular library for ML research. DIMOS implements essential algorithms to perform MD and MCMC simulations, providing an easy-to-use way to interface MLIPs and an efficient implementation of classical force field components in addition to implementations of common integrators and barostats. Additional components are the efficient calculation of neighborlists and constraint algorithms which allow for larger timesteps of the numerical integrator. By relying on PyTorch, we inherit many advances achieved by the ML community: We achieve fast execution speed on diverse hardware platforms, combined with a simple-to-use and modular interface implemented in Python.

In particular, automatic differentiation, a cornerstone of ML, allows for novel approaches by enabling the auto-

matic calculation of derivatives of arbitrary components in the computation graph. For example, differentiating through the simulation either to tune force-field parameters based on desired dynamic properties [6] or to adapt the parameters of simulation methods to accelerate the sampling in equilibrium [7] becomes possible, representing only a small subset of potential future developments.

DIMOS fills an important void in the landscape of existing differentiable simulation frameworks which currently suffer from critical limitations. For example, torchMD [8] does not implement neighborlists and thus becomes computationally prohibitive for larger systems, and JAX M.D. [9] does not implement classical force field. While there exist separate implementations for many of the algorithms implemented in DIMOS in various code bases, there currently exists no unified and reliable simulation framework for them [10].

In the remainder of the manuscript, we establish: *a*) The ease of use and modularity of the framework, *b*) the performance of the framework for molecular dynamics simulations, and *c*) showcase of the end-to-end optimization capabilities of the framework by optimizing Monte Carlo proposal distributions.

I. RESULTS

Setting up a minimal simulation in DIMOS can be done in only a few lines:

```
system = dimos.AmberForceField("config.prmtop")
integrator = dimos.LangevinDynamics(dt, T, gamma,
    system)
simulation = dimos.MDSimulation(system, integrator,
    positions, T)
simulation.step(num_steps)
```

Here, a molecular system configuration from a common

* henrik.christiansen@neclab.eu

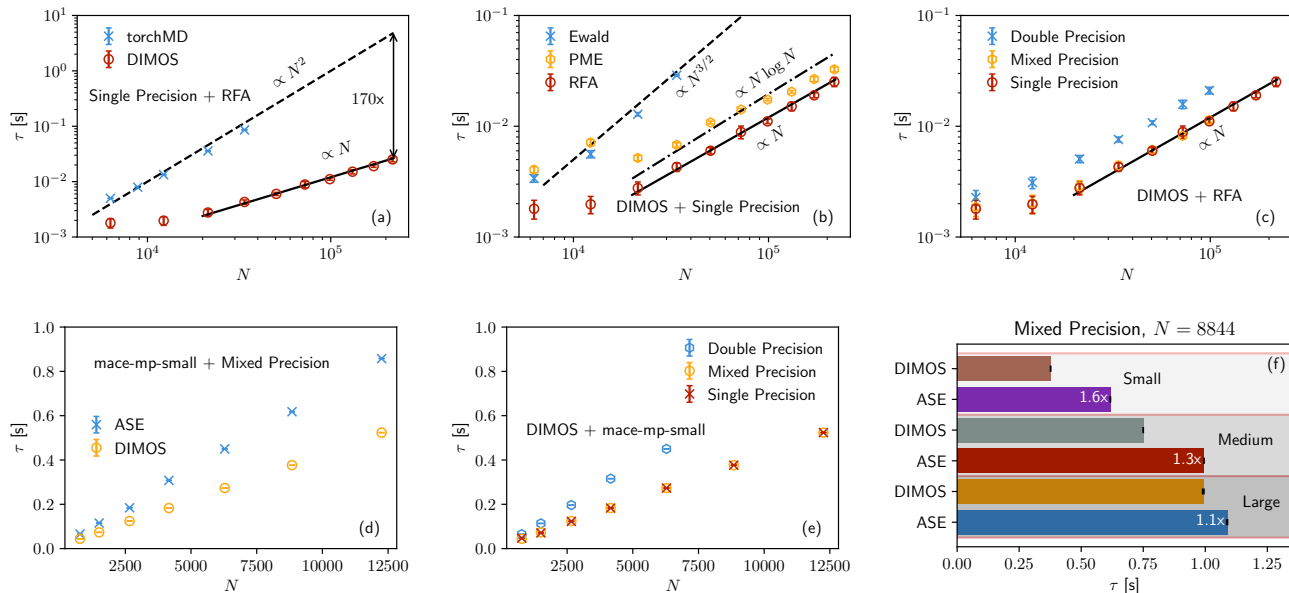


FIG. 1. **Computational Performance Analysis:** Runtime τ in seconds per MD step for a water box with constant density as a function of number of atoms N . (a) Shows the runtimes for torchMD and DIMOS using single precision numerics and RFA to model the electrostatic interactions: Runtimes are presented for DIMOS using single precision numerical accuracy. In (c), we investigate the effect of the chosen computational precision on the runtime, modelling electrostatic interactions via RFA in DIMOS. In all cases, the lines indicate the theoretically expected asymptotic computational complexity. (d)-(f) Show the performance of running the MACE foundation model, where in (d) we compare the runtimes of DIMOS to ASE using the small MACE model and mixed precision for different N , and (e) investigates the influence of choosing different numerical precision within DIMOS. (f) Presents the runtimes for the biggest system that can be simulated using the large MACE model ($N = 8844$) and compares the resulting τ for DIMOS and ASE.

input format is loaded and an integrator object to perform Langevin dynamics is initialized, which combined form the simulation; we then run the simulation for a given number of steps. All other required functions are hidden to the user, such as the handling of boundary conditions or neighborlists, but they are still easily accessible for inspection or extension. Due to the modular setup of the framework and since we are relying only on two external dependencies (PyTorch [5] to implement the simulation and `parmed` [11] to read configuration files), it is straightforward to develop novel approaches, a unique strength of our package.

In the following section, we present the resulting runtimes of DIMOS for simulations of water boxes to probe the influence of system size and simulation/modelling choices such as the method to calculate long-range interactions or different schemes for the numerical datatypes for classical force fields and MLIPs. Then we turn towards the simulation of proteins in explicit solvent, investigating the influence of constraints on the simulation speed and presenting ML/MM as hybrid solution. Finally, we demonstrate how the end-to-end differentiability of the code base allows us to differentiate through the whole simulation to tune parameters of the simulation and system in the framework of Hamiltonian Monte

Carlo (HMC) [12, 13].

A. System-size Scalability

We investigate the runtimes per simulation step averaged over several simulation steps for water boxes of fixed density with varying number of atoms N . In Figs. 1(a)-(c), we present the average runtime per MD step τ as a function of number of atoms N in an unconstrained simulation under Langevin dynamics at 300 K with timestep $\Delta t = 0.5$ fs, friction coefficient $\gamma = 0.1$ fs $^{-1}$, and cutoff $r_c = 10$ Å. The water is modeled by the TIP3P water model [14].

In (a) we compare τ obtained in DIMOS to torchMD [8] for simulations running in single floating point precision and electrostatic interactions modeled by the reaction field approximation (the RFA is the only setup for electrostatics supported by torchMD). We observe linear scaling of the runtime per step t in DIMOS, whereas torchMD displays quadratic scaling as a function of number of atoms N . For the largest system size tested ($\approx 300,000$ atoms), DIMOS achieves a 170 \times speed-up over torchMD. This extrapolation is based on torchMD's quadratic complexity, while we show that DIMOS maintains linear scaling due to neighborlists. For a fair com-

```

ml_atoms = [...] # Indices of atoms that are being modeled by ML system.
mm_system = dimos.GromacsForceField("config.top", "config.gro", excluded_bonded_atoms=ml_atoms)
ml_system = mm_system.as_mace_system("mace-mp-large", atom_range=[0, len(ml_atoms)])
mlmm_system = dimos.mlmm.MLMMsystem(ml_atoms, ml_system, mm_system)

```

(a) Example code showing how to set up a simulation of an ML and ML/MM modeled system starting from an MM description.

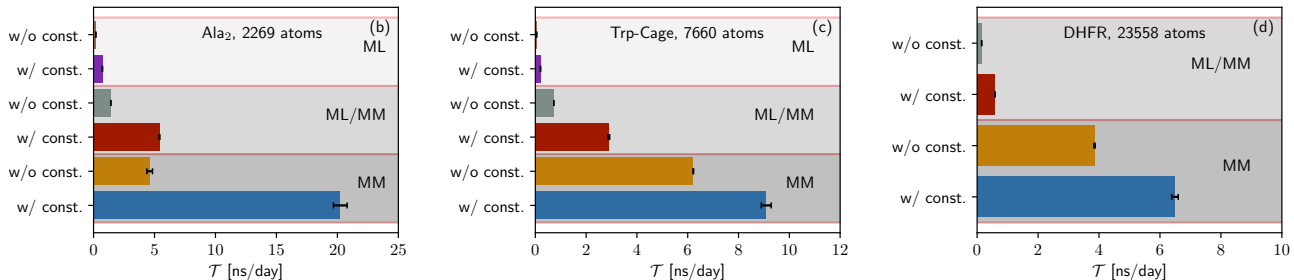


FIG. 2. **Simplicity of Use and Acceleration for Proteins:** (a) Demonstration on how to set up both classically and machine-learning enhanced systems in DIMOS. `ml_atoms` specifies which atoms should be modeled by the MLIP system, and also can be empty in case one does not want to model any systems using ML. (b-d) Achievable simulation time per day \mathcal{T} with and without constrained motion of the hydrogens for each of the three cases of a system modeled purely by ML, the hybrid approach using ML/MM, and a purely MM based modelling. In all cases, the MLIP model was chosen to be `mace-mp-large`. In (b), we present the data for alanine-dipeptide (Ala₂), (c) shows Trp-Cage, and (d) shows dihydrofolate reductase (DHFR). All systems are modeled using explicit water modeled by the TIP3P parameters [14]. In (d), the biggest system, it is not possible to model purely with ML, as for this system size the MLIP model required more than the available GPU memory.

parison, we check the validity of the neighborlist after every integration step, avoiding any potential artifacts leading to inaccuracies in the force/energy evaluation.

Panel (b) demonstrates the influence of different methods how to model electrostatics within DIMOS. We use single precision numerics. Clearly the RFA is the fastest option due to the simple mean-field treatment of charges outside the cutoff. Somewhat slower, but still competitive is the particle-mesh Ewald (PME) [15] method, for which one expects $O(N \log N)$ complexity, which roughly captures our data. In contrast, using direct Ewald summation [16] with theoretically ideal complexity $O(N^3/2)$ is significantly slower already for medium-sized systems, and can only provide a minor performance improvement over PME for small systems. In addition, direct Ewald summation requires significantly more GPU memory and can thus not be used for large systems.

The influence of the chosen numerical accuracy is presented in Fig. 1(c) with electrostatic interactions modeled by RFA, where we find that double precision as expected is overall slower on our employed GPU. Very little performance penalty is observed using mixed precision, where the integration is performed in double precision, but the force/energy evaluation is performed in single precision. However, this approach cannot be used for larger systems, as the memory requirements increase significantly. If memory consumption is not a bottleneck, it is advisable to always consider using mixed precision due to the reduction of accumulation of errors in comparison to single precision, where such effects can be detrimental.

In Figs. 1(d)-(f) we investigate the behavior of DIMOS in conjunction with MLIPs by simulating the same wa-

ter boxes as in (a)-(c) with the `mace-mp` foundational model [17, 18]. MACE is a state-of-the-art equivariant message-passing graph neural network that models interatomic interactions. The simulation parameters remain largely the same, however, we now employ the standard interaction cutoff for message passing of $r_c = 3 \text{ \AA}$ in MACE. The runtimes are here compared to ASE [19], the de-facto (non-differentiable) standard approach in many situations for running MLIP based simulation due to its simplicity. We observe in (d) that for the smallest foundation model `mace-mp-small`, DIMOS displays a significant increase in speed using mixed precision (as also implicitly employed in ASE). As shown in (e), there is virtually no penalty in using mixed precision for simulations using MLIPs. This is because the runtime and memory consumption is dominated by the ML model, so that all other factors effectively become negligible, at least for the currently achievable system sizes.

Figure 1(f) shows the influence of choosing different sizes of the `mace-mp` model in comparison between DIMOS and ASE for the biggest system size ($N = 8844$) that can be simulated using all ML model sizes. For the small model, the speed-up obtained by DIMOS is the biggest with factor $1.6\times$, i.e., nearly half of the time in ASE is spent in integrating the equation of motion and memory transfer. For the bigger models, the difference between DIMOS and ASE become less pronounced due to the larger time spent in the actual ML model evaluation, but the speed-up still remains sizable.

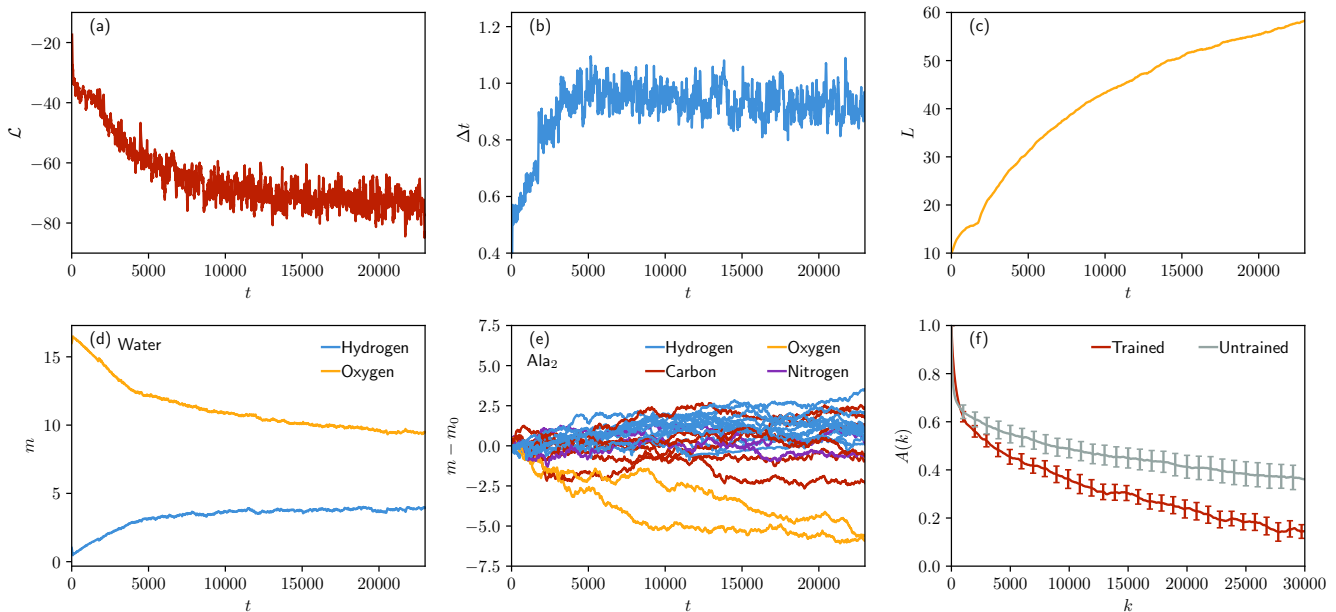


FIG. 3. **End-to-end Optimization:** Plots demonstrating the end-to-end learning of simulation parameters for HMC. (a) Loss \mathcal{L} as function of training time t . (b),(c) The timestep Δt and number of integration steps L against training time t . (d),(e) The behavior of the masses m for (d) the hydrogen and oxygen atoms in the water molecules, optimized as shared parameter between all molecules and (e) the remaining masses in Ala₂. In (e) we plot $m - m_0$ to better highlight the relative change of masses for the diverse atom types. (f) Autocorrelation function $A(k)$ of the potential energy $U(x)$ as function of lag-time k measured in terms of the number of energy evaluations.

B. Constraints and Hybrid ML/MM for Protein Systems

We simulate three benchmark systems of varying size: *i*) Alaninedipeptide (Ala₂) with 2269 atoms, *ii*) Trp-Cage with 7660 atoms, and *iii*) dihydrofolate reductase (DHFR) with 23558 atoms. The first two systems are standard test-systems to probe novel simulation methods, and the latter is a common test-system from the joint AMBER/CHARMM benchmark [20]. Since we here also want to probe the effect of using constraint algorithms to increase the timestep on the achievable simulation time, we shift our metric to the simulation time achievable per wall-clock day \mathcal{T} , i.e., how many ns of simulation can be achieved per day, to evaluate the performance of DIMOS. We implement a combination of SETTLE [21] and CCMA [22] to constrain the relative position of all water molecules and all other bonds involving one hydrogen atom (for details, see Methods section III E 4). In the simulations we use the Nosé-Hoover integrator with collision frequency of 0.05 fs^{-1} and $\Delta t = 0.5 \text{ fs}$ timestep for disabled constraints, and $\Delta t = 2.0 \text{ fs}$ timestep with constraints enabled.

For the protein systems, we are considering three scenarios: The system purely modeled by `mace-mp-large` (ML), a hybrid approach where the protein is modeled by the MACE model (ML/MM), but the water is parameterized by the classical TIP3P water model [14], and a fully

classical simulation using AMBER99SB [23] force field and TIP3P water (MM) [14]. In the ML and ML/MM case, electrostatic contributions are ignored (DIMOS implements several options), whereas in the MM case we use PME. As demonstrated in Fig. 2(a), it is straightforward to set up systems modeled by the three options in DIMOS. The only option to be specified by the user is which MLIP to use, and which atoms should be modeled by it.

In Fig. 2(b), we present the data for Ala₂ using the three approaches with and without constraints. For the systems modeled by ML or ML/MM, we adopt the constraints as defined for the MM system. The ML approach is clearly the slowest option with $\mathcal{T} \approx 0.18 \text{ ns/day}$ of simulation time without constraints. This is in contrast to the fastest simulation time $\mathcal{T} \approx 20 \text{ ns/day}$ (more than $100\times$ faster than the ML approach), achieved by modelling the interaction using MM and with constraints activated. As viable alternative, one may consider the hybrid approach, where with constraints we achieve $\mathcal{T} \approx 5.4 \text{ ns/day}$.

For the larger Trp-Cage system presented in (c), the differences become even more pronounced. While a classical ML simulation without constraints achieves $\mathcal{T} \approx 0.05 \text{ ns/day}$, the ML/MM approach without constraints is $14\times$ faster. In the extreme case, employing constraints and modelling all interactions using MM, we observe a speed-up of $> 175\times$. While naturally modelling a part or all of the interactions using MM comes with an accuracy penalty, this highlights the strength of DIMOS as

a modular framework with easy combination of various techniques tailored to the problem.

Figure 2(d) shows the performance for DHFR, which due to memory constraints of MACE could not be simulated completely using the ML approach. Using ML/MM, we obtain runtimes in the range of ≈ 0.15 to $\mathcal{T} \approx 0.6$ ns/day for the ML/MM approach, and ≈ 3.8 to ≈ 6.5 ns/day for the pure MM modelling. This means that, in regions with increased accuracy requirements, it is now possible with DIMOS to simulate these systems with only a $\approx 10\times$ performance penalty over purely MM modelling.

C. End-to-end Optimization of Hamiltonian Monte Carlo

We utilize the end-to-end differentiability of DIMOS to optimize the proposal distribution in MCMC simulations. HMC constructs proposal configurations that are informed by the forces acting on the particles, in contrast to random-walk MCMC where proposals are uninformed. This allows for large configurational changes without incurring a low acceptance rate. For more details on HMC and the learning setup, see Method section III F.

The performance of HMC crucially depends on the choice of simulation parameters, where suboptimal choices can lead to a significant increase in autocorrelations between samples. We optimize three classes of parameters critical to the efficiency of HMC: The integration timestep Δt , the number of integration steps L , and the atomic masses m_i . The loss function \mathcal{L} promotes large configurational changes while maintaining reasonable acceptance rates, balancing exploration and computational effort (for details, see Section III F). Figures 3(a)-(e) present \mathcal{L} , Δt , L , and the atomic masses m_i during training for a system of Ala₂ in explicit solvent modeled by the classical force field AMBER99SB [23] and TIP3P water [14]. We clearly see that the loss \mathcal{L} decreases as a function of training time t , and reaches a plateau towards the end. The timestep increases from the small starting value of to $\Delta t \approx 1$ fs, which is significantly larger than the 0.5 fs timestep allowed by the physical dynamics in MD. In conjunction with the large number of integration steps of $L \approx 60$, this corresponds to big configurational changes for each proposal.

The masses of atoms in the water molecules are optimized for as shared parameters between all molecules. As shown in Fig. 3(d), we find that the hydrogen masses are increased while the masses of the heavy oxygen atoms are decreased, similar to what is done manually in MD simulations [24]. A similar trend can be observed in Fig. 3(e) for Ala₂, however, with smaller relative changes in the atom masses.

In Fig. 3(f) we plot the autocorrelation function A of the potential energy as function of lag time k measured in the number of energy evaluations for a simulation where the parameters are fixed to the optimized ones. We find

that, compared to a simulation with typical parameters of $\Delta t = 0.5$ fs and $L = 10$ without mass repartitioning shown in the same plot, the autocorrelations decay significantly faster in the optimized case. This translates to an exponential autocorrelation time (as measured in computational effort) of $\tau_{\text{exp}} \approx 13,150$ in the trained case versus $\tau_{\text{exp}} \approx 38,900$ in the case where the simulation parameters are chosen ad-hoc, corresponding to a $\approx 3\times$ speed-up in sampling.

II. DISCUSSION

In this work, we have introduced DIMOS, an end-to-end differentiable simulation framework. Our results demonstrate that our framework not only extends the capabilities of conventional non-differentiable MD packages, but also provides a modular platform for implementing emerging methodologies in molecular simulations. Compared to prior approaches, our work bridges the gap between validated general-purpose simulation tools and the specialized needs of ML-enhanced modelling, allowing researchers to explore novel approaches that were previously computationally prohibitive.

We have shown that DIMOS has superior performance compared to other fully differentiable simulation frameworks, with a speed-up factor of up to $170\times$. Ewald and particle-mesh Ewald summation are implemented as advanced approaches to calculate electrostatic interactions, allowing also for the gradient-based optimization of MLIPs based on them. The mixed precision implementation allows for accurate evolution in time without substantial overhead in computational effort.

Simulations using MLIPs are significantly accelerated using DIMOS, with speed-up of $\approx 1.6\times$ over ASE. Another strength of DIMOS is demonstrated for three protein systems in explicit solvent, for which we implement a hybrid approach combining classical force fields and MLIPs. We find that this accelerates the simulations significantly over pure MLIP based modelling. Additional speed-up is achieved by constraining the movement of fast oscillating atoms, allowing for a $4\times$ increased timestep compared to unconstrained dynamics. By optimizing end-to-end the parameters of HMC and introducing a data-driven way to perform mass-repartitioning, we are able to obtain a $\approx 3\times$ acceleration in sampling efficiency over ad-hoc chosen simulation parameters.

DIMOS is designed to become a vital tool for researchers in computational physics, chemistry, and biology, combining the modularity needed for method development with good simulation performance. Due to the modular framework, it is straightforward to add additional features which may be needed in those communities, such as for example the support for more general simulation boxes or virtual particles.

III. METHODS

We generally aim to reproduce the behavior of OpenMM [26] and check, whenever possible, consistency with regard to their implementation both for static and dynamic properties.

In the first part of the method section, we present the different approaches to model interatomic potentials in DIMOS. This first part will focus on classical force fields, in which a relatively simple and heuristic functional form is assumed to describe the interactions of the atoms, with explicit consideration of covalent bonds. In contrast, MLIPs typically do not consider explicit information of covalent bonds and instead often rely on learning the interactions based on generalized higher order terms. Finally, due to considerations of simulation speed, it may turn out to be beneficial for some systems to model part of the interactions classically, and another part using MLIPs. A schematic depiction of the three approaches is presented in Figs. 4(a)-(c), where for the depiction of the interaction via MLIPs a graph neural network with message-passing approach was considered.

The other parts of the Methods section present details related to the handling of the dynamical evolution of the system, such as integrators and constraints. Finally, we provide the details of the self-tuning HMC approach.

All simulations in the three benchmark simulation frameworks (DIMOS, OpenMM, ASE) for which we quote runtimes were performed using an NVIDIA RTX 6000 Ada GPU with 48GB memory on a server equipped with an Intel Xeon Gold 5412U CPU with 24 cores and 256GB memory.

A. Classical Force Fields

In classical molecular mechanics modelling of a system, one distinguishes between non-bonded and covalently-bonded atoms, where the former interactions are composed of pair-wise potentials of van der Waals type and electrostatic Coulomb interactions. The interaction between bonded atoms, in addition to a pair-wise type potential between atoms, is modeled by introducing higher-order interactions. Some force-field parameterization additionally include corrections which are based on tabular definitions of interaction energies between four atoms, called energy correction map (CMAP) [27]. We implement the energy components needed to reproduce the most common parameterizations of AMBER [23] class force fields, and some additional components often used in CHARMM type parameterizations [27]. Fig. 4(d) schematically displays typical energy components of classical force fields, which we have implemented in DIMOS and will present in more details in the following.

1. Bonded Interactions

The interaction between two atoms i and j that are covalently bonded is modeled by a simple harmonic potential

$$U_{\text{bonded}}(i, j) = k_{ij}(r_{ij} - r_{ij}^0)^2 \quad (1)$$

where $r_{ij} = |\vec{r}_{ij}|$ is the Euclidean distance between the atoms, k_{ij} models the interaction strength and r_{ij}^0 is the equilibrium or target distance. Usually, k_{ij} and r_{ij}^0 depend on the atom types involved in the bond and not explicitly on the particular atom, but we still use this more general notation for simplicity.

For pairs of three atoms i , j , and l , linked sequentially by covalent bonds, one likewise defines a harmonic potential, which now depends on the angle between the atoms

$$U_{\text{angle}}(i, j, l) = k_{ijl}(\theta_{ijl} - \theta_{ijl}^0)^2 \quad (2)$$

where using the unit vector $\hat{r}_{ij} = \vec{r}_{ij}/|\vec{r}_{ij}|$ one defines $\theta_{ijl} = \arccos(\hat{r}_{ij} \cdot \hat{r}_{lj})$ as the angle between the three atoms, and the other parameters are defined in analogy to the harmonic bonded potential. For some force-fields, the three-body interactions are described by the Urey-Bradley potential, which is a combination of above angle and bond potentials.

Interactions between four sequentially bonded atoms i, j, l, m can be described by a torsion potential

$$U_{\text{torsion}}(i, j, l, m) = \sum_n k_{ijlm}^n [1 + \cos(n\omega_{ijlm} - \omega_{ijlm}^0)] \quad (3)$$

where ω_{ijlm} is the dihedral angle between the two planes spanned by i, j, l and j, l, m and n specifies the multiplicity. The other parameters are defined in analogy to the previous two contributions. For the torsion parameters, one distinguishes between proper and improper dihedral angles, differing whether the involved atoms are in a chain or not. Alternatively, some force fields simply model the improper dihedrals harmonically.

Implementing new energy contributions similar to the ones above is straightforward in DIMOS, demonstrating a key advantage of our package. The only requirement is that any new class accepts the positions of the system as input and returns the final energy, see our example implementation of `calc_energy` for the harmonic bond potential:

```
def calc_energy(self, pos):
    distances = get_distances_edge_list(
        pos, self.bond_list, self.periodic, self.box)
    return torch.sum(self.bond_parameters[:, 0] *
                    (distances - self.bond_parameters[:, 1])**2)
```

Here, `get_distances_edge_list` takes care of returning the distances respecting periodic boundaries of the atoms defined in the `self.bond_list`. The parameters of the potential are stored in `self.bond_parameters`, which is handed over at initialization of the class.

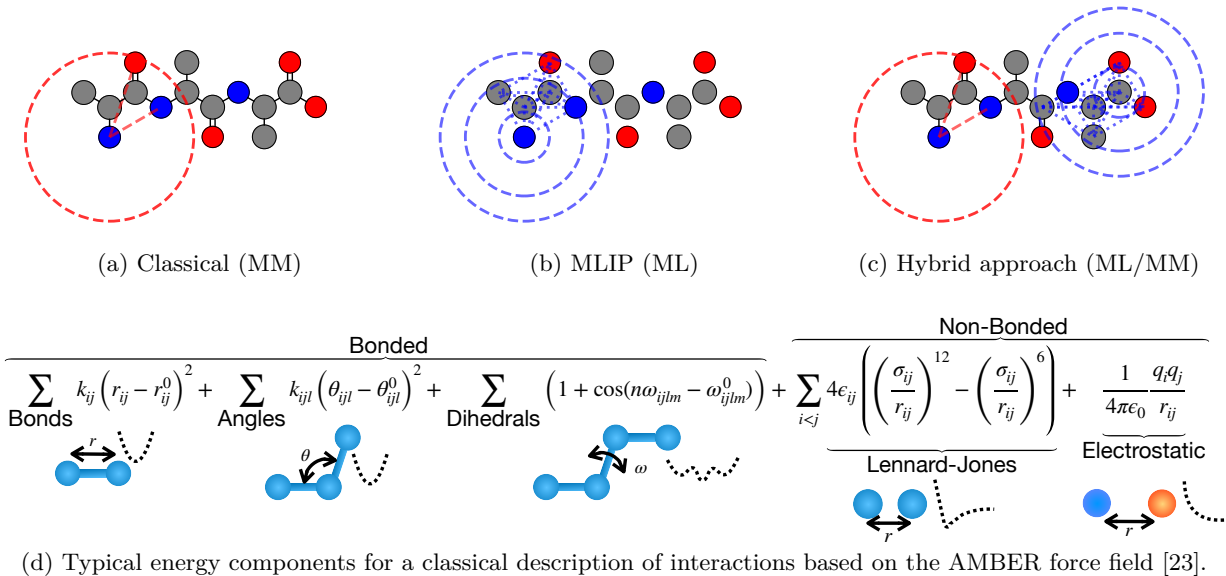


FIG. 4. **Schematic Visualization:** In (a)-(c) a schematic representation of Alanine tripeptide (Ala_3), where the atomic interactions are modeled (a) solely classically (MM), (b) solely using an MLIP (ML), or (c) using a hybrid approach (ML/MM). The red circle marks a region modeled by a classical force field, where one defines interaction terms based on covalent bonds and non-covalently bonded atoms. The blue circles represent the message passing iterations of a graph neural network used to construct many-body interactions, for details see Ref. [25] and the references therein. In all cases, only the operations based on calculating the force/energy for a single atom are depicted, and for a full evaluation the steps are repeated for every atom. In (d), the energy components for a classical force field are depicted, based on the parameterization of AMBER class interactions [23]. Covalently bonded and non-bonded interactions are distinguished, with exclusions in the non-bonded interactions for directly or indirectly bonded atoms. For more details on the individual contributions, see Section III A.

2. Nonbonded Interactions

In a usual simulation, the most time consuming part of the calculations is related to the non-bonded atoms of the system. *A priori*, all atoms interact with each other, leading to $O(N^2)$ complexity for the computations. For methods using synchronous dynamics, such as MD simulations, one routinely relies on heuristic cut-offs, where for non-integrable interactions one performs the computation both in real and reciprocal space, leading to an improved convergence [28].

The introduction of a cut-off allows one to use specialized data structures to store pairs of atoms that are within the interaction radius of each other, so-called neighborlists (more generally called edge lists in the ML literature). In the following, we will discuss the components of neighborlist and their implementation in DIMOS. After this, the two main non-bonded energy contributions of classical force fields are discussed.

a. Neighborlists In DIMOS, we employ a combination of Verlet neighborlist [29] and cell lists [30] to construct the Verlet lists. Neighborlists are a data structure in which one simply stores all pairs of atoms that are within a distance $r_{\text{nl}} = r_c + r_g$, where r_c is the cutoff distance of the potential, and r_g is the so-called ghost radius [29] (set to $0.25r_c$ by default in DIMOS). This implies that the list contains more atom pairs than strictly

needed for the computation of the interactions and one wastes some computation when calculating the distance r for all pairs with $r_{\text{nl}} > r > r_c$. However, this is more than compensated by being able to reuse the neighborlist more than once during the simulation, because each atom only moves a relatively small distance at each iteration. Due to the introduction of the ghost radius r_g , the pair list only loses its validity whenever a single atom has moved a distance d greater than half the ghost radius $d > r_g/2$ since construction of the list. Only then, the neighborlist needs to be reconstructed. This reduces the complexity to $O(N)$ per synchronous update of all atoms whenever the neighborlist is valid, in contrast to an $O(N^2)$ complexity otherwise.

However, a naive re-construction of the neighborlist still has $O(N^2)$ complexity, ultimately not improving the complexity of the simulation. This is because the distance between all pairs of atoms needs to be calculated to decide which ones are below r_{nl} . An alluring solution to this problem is the partitioning of the simulation box into cells based on the spatial coordinates of the atoms. Each cell is chosen to be of at least r_{nl} length, and each atom is assigned to one of the cells. Then, to find all atom pairs within r_{nl} , one simply needs to check the neighboring cells (including off-diagonal neighbors) and store all combinations of atoms within the neighborlist. The overall complexity of the algorithm is $O(N)$.

By default, the end-user of DIMOS intending to run a simulation does not need to explicitly consider the use of neighborlists, since these are automatically been utilized and kept up-to-date. For some applications, as for example training an MLIP on some pre-existing data, one can obtain the atom pairs as

```
nb_handling = dimos.NeighborHandling(periodic,
    num_atoms, cutoff, box, exclusions)
nblast = nb_handling.get_neighborlist(pos)
```

In case the boundary conditions are not periodic, the system is, for the sake of neighborlist computation, embedded into a non-periodic box. For this new (virtual) box, the usual routines are called without wrapping around the coordinates of the cells as would be otherwise necessary with periodic boundaries.

b. Van der Waals and Coulomb interactions One of the most used functions to model van der Waals interactions is the 12–6 Lennard Jones potential

$$U_{\text{LJ}}(r_{ij}) = 4\epsilon_{ij} \left(\left(\frac{\sigma_{ij}}{r_{ij}} \right)^{12} - \left(\frac{\sigma_{ij}}{r_{ij}} \right)^6 \right). \quad (4)$$

The parameters ϵ_{ij} and σ_{ij} are determined from atom specific parameters ϵ_i and σ_i by combining rules as

$$\epsilon_{ij} = \sqrt{\epsilon_i \epsilon_j}, \quad \sigma_{ij} = \frac{\sigma_i + \sigma_j}{2}. \quad (5)$$

To avoid non-smooth behavior at the cutoff r_c , one can adapt different schemes. We here follow the approach of OpenMM [26] and apply the switching function

$$S(x) = 1 - 6x^5 + 15x^4 - 10x^3, \quad (6)$$

to Eq. (4), where $x = (r_{ij} - r_s)/(r_c - r_s)$ and $r_s < r_c$ is the switching distance. For simulations at constant temperature and pressure in the NPT ensemble, we have also implemented long-range dispersion corrections that approximate the contributions beyond r_c [31].

The coulomb potential used to model electrostatic interactions is given by

$$U_{\text{el}}(r_{ij}) = \frac{1}{4\pi\epsilon_0} \frac{q_i q_j}{r_{ij}}, \quad (7)$$

where ϵ_0 is the vacuum permittivity and q_i is the (partial) charge of atom i . Similar to the Lennard-Jones case, it is possible to introduce a direct cutoff in real space. This approach is referred to as the reaction field approximation [32] (RFA) which modifies Eq. (7) to read

$$U_{\text{RFA}}(r_{ij}) = \frac{1}{4\pi\epsilon_0} q_i q_j \left(r_{ij}^{-1} + k_{\text{RFA}} r_{ij}^2 - c_{\text{RFA}} \right) \quad (8)$$

with $k_{\text{RFA}} = r_c^{-3}(\epsilon_s - 1)/(2\epsilon + 1)$ and $c_{\text{RFA}} = 3\epsilon_s r_c^{-1}/(2\epsilon + 1)$, where ϵ_s is the dielectric constant of the solvent. This approach thus approximates the influence of the atoms outside the cutoff in a mean-field manner, and may thus introduce uncontrolled effects.

A less heuristic method to introduce a cutoff in electrostatic modelling is Ewald summation [16], for which one writes

$$U_{\text{Ewald}}(r_{ij}) = U_{\text{dir.}}(r_{ij}) + U_{\text{recip.}}(r_{ij}) + U_{\text{self}} \quad (9)$$

with

$$U_{\text{dir.}} = \frac{1}{2} \sum_{i,j} \sum_{\vec{n} \in \mathbf{n}} q_i q_j \frac{\text{erfc}(\alpha|\vec{r} + \vec{n}|)}{|\vec{r} + \vec{n}|} \quad (10)$$

$$U_{\text{recip.}} = \frac{1}{2\pi V} \sum_{i,j} \sum_{\vec{k} \in \mathbf{k} \neq 0} \frac{\exp(-(\pi\vec{k}/\alpha)^2 + 2\pi\vec{k} \cdot \vec{r}_{ij})}{\vec{k}^2} \quad (11)$$

$$U_{\text{self}} = -\frac{\alpha}{\sqrt{\pi}} \sum_i q_i^2. \quad (12)$$

The potential is thus split into a real space contribution $U_{\text{dir.}}$, a reciprocal space contribution $U_{\text{recip.}}$, and the self energy U_{self} . The sums $\sum_{\vec{n} \in \mathbf{n}}$ and $\sum_{\vec{k} \in \mathbf{k} \neq 0}$ run over all periodic copies of the system, respectively, all reciprocal vectors. V is the volume of the box, and α controls the shift between $U_{\text{recip.}}$ and U_{self} .

By construction, the sums of the individual energy contributions in real and reciprocal space converge significantly faster than directly evaluating the sum. Hence, it becomes possible to choose a much smaller cutoff for both sums to reach a target accuracy, significantly reducing the number of necessary computations.

For an ideal choice of cutoff of the real and reciprocal summation as well as crossover parameter α , it can even be shown that this reduces the computational effort from $O(N^2)$ to $O(N^{3/2})$ per step. Note that for any choice of α above formulas are correct; hence, the choice of α only influences which cutoff r_c and k_c can be chosen for a desired accuracy. In practice, α is by default heuristically determined from the prescribed tolerance δ and a fixed cutoff r_c (typically the one used for the van der Waals interactions) as [26]

$$\alpha = \sqrt{-\log 2\delta}/r_c. \quad (13)$$

Then, one uses a root-finding algorithm to determine k_c via the empirically found relation

$$\delta = \frac{k_c \sqrt{d\alpha}}{20} \exp(-(\pi k_c / d\alpha)^2). \quad (14)$$

To further speed-up computation, it is possible to carry out the reciprocal sum using a fast Fourier transform (FFT) by distributing the charges onto a lattice via spline interpolation. This significantly speeds up the calculation of $U_{\text{recip.}}$, and the overall complexity also reduces to $O(N \log N)$. Following OpenMM [26], we implement smooth PME [15]. For this, we also implement B-splines [33] based on the recursive definition of the splines, resulting in custom forward and backward implementation within PyTorch. The number of nodes in the mesh is chosen heuristically as $n_{\text{mesh}} = 2\alpha d / 3\delta^{1/5}$, where α is again determined from Eq. (13).

c. Exclusions and Exceptions Atoms that are directly bonded or indirectly bonded to each other are excluded from the non-bonded energy terms. In addition, atoms connected via three bonds (such as in torsion contributions) are often treated differently. The most common way to handle these 1-4 exceptions is to scale the strength of the non-bonded interactions by some common factor < 1 . Alternatively, some parameterizations of force-fields scale each exclusion by an individual factor. In DIMOS, exclusions and exceptions are handled at the level of neighborlists, where excluded interaction pairs are filtered out. Since all possible 1-4 exceptions are known at simulation setup, they are handled explicitly by the non-bonded interaction method.

B. Machine Learning Based Descriptions of Intermolecular Interactions

MLIPs do not typically introduce an explicit distinction between non-bonded and bonded atoms, and instead often build higher-order interactions between all atoms within a cutoff distance using various approaches, see Ref. [25] and references therein. Usually, these approaches include physical features in some capacity, for example a large body of work only considers features that are invariant to rotations and translations of the system and uses rather standard ML architectures with learnable parameters [34]. Another line of work explicitly constructs the architectures such that their internal features or their output transform equivariantly to the input, i.e., for example rotating the system also leads to a predictable rotation of the output [17, 35, 36].

We implement the interface to two current state-of-the-art MLIP models: MACE [17] and ORB [35]. We want, however, to stress that DIMOS makes no explicit assumption on the model and is rather agnostic to the details, as long as the models are implemented in `PyTorch`. In Fig. 4(b) we schematically demonstrate the basic setup of message-passing graph neural network MLIPs, in which many-body interaction terms are built using successive message passing iterations. However, since we do not implement any novel MLIP architecture in DIMOS, we refer to the literature on details as well as advantages/disadvantages of the respective approaches [25, 37].

Using DIMOS, the best performance is achieved if the model expects a combination of the neighborlist, distance vectors or distances, and/or shifts, since they are calculated anyway in DIMOS and recalculating (some of them) within the model leads to wasted calculations. By having the full simulation framework implemented in `PyTorch`, it is possible to compile parts or the whole simulation. This also extends to compiling MLIPs using `torch.compile`, which is currently not possible when using LAMMPS [38] or OpenMM [26] to interface the MLIP. Setting up a system modeled by a (foundational) MACE model can be achieved in a single line:

```
ml_system = dimos.MaceFoundationalSystem(masses,
                                         atomic_numbers)
```

In addition, there are some optional parameters, which, however, are not necessary in general. This highlights the simplicity of using DIMOS to run fast and scalable simulations using an MLIP, compared to other established approaches requiring a vast number of steps.

MACE is currently one of the most prominent MLIPs in the literature [17], with diverse applications in different domains. We specifically employ the MACE material project foundation model (`mace-mp`) [18], which is available in the `small`, `medium`, and `large` variant depending on the chosen parameterization. In DIMOS, we support the acceleration of MACE using NVIDIA cuEquivariance [39], and activate it in all our benchmarks.

C. Machine Learning/Molecular Mechanics

An alternative to describing the system fully using an MLIP is to employ a hybrid approach, where part of the system is described using an MLIP, and the remaining part by a classical force field. This is often called ML/MM, standing for machine learning/molecular mechanics, a term derived from QM/MM used to describe the combination of quantum mechanical *ab initio* calculations and molecular modelling. While the field of QM/MM is quite advanced, in particular in choosing a proper embedding approach for the electrostatic interactions [40], it is significantly less explored for the ML/MM approach. The current approaches are based on a mechanistic embedding, and as such the electrostatic interactions are treated on the MM level [41] or ignored. To define an ML/MM system, one defines a `ml_system` which is modeled with an MLIP and a `mm_system` described by a classical force field. In addition, one needs define `ml_atoms`, a list containing the atom indices modeled by the `ml_system`, which then results in the new combined system. Example code on how to achieve this is presented in Fig. 2(a).

D. Handling of Units

In DIMOS, we do not choose a specific unit system to perform all calculations, but rather directly set the necessary constants in the chosen unit system. This has the big advantage over established approaches, that the computations are very interpretable, which can be beneficial when testing against established simulation packages which may use different unit systems. In particular, for “unitless” simulations as often performed in statistical physics, this allows for an effortless comparison to many specialized code bases not using units. In most cases the units in DIMOS are adopted from the AMBER simulation suite, unless otherwise specified. Globally changing

the unit system is straightforward and can be achieved by calling

```
dimos.init_constants_in_unit_system(unit_system)
```

where `unit_system` is the target unit system encoded as string, accepting both names of specific simulation packages or energy units.

E. Molecular Dynamics and Energy Minimization

With the system description in place, we now present the implemented methods that update the position of the atoms, with various goals in mind.

1. Molecular Dynamics

The basis of MD is numerically solving Newtons equation of motion given by $\frac{\partial E}{\partial \vec{r}} = -\vec{F} = -m\vec{a}$. To do so, we implement the ubiquitous methods by Verlet [29] in its velocity variant [42], which numerically integrates Newtons equation in time and hence conserve the total energy of the shadow Hamiltonian.

An MD simulation utilizing the velocity Verlet integrator consists of the following steps:

1. Update velocities: $\vec{v}_i(t + \frac{1}{2}\Delta t) = \vec{v}_i(t) + \frac{1}{2}\vec{a}_i(t)\Delta t$.
2. Update positions: $\vec{x}_i(t + \Delta t) = \vec{x}_i(t) + \vec{v}_i(t + \frac{1}{2}\Delta t)\Delta t$.
3. Apply position constraints.
4. Calculate $\vec{a}_i(t + \Delta t)$.
5. Perform second velocity update:
 $\vec{v}_i(t + \Delta t) = \vec{v}_i(t + \frac{1}{2}\Delta t) + \frac{1}{2}\vec{a}_i(t + \Delta t)\Delta t$.
6. Apply velocity constraints.
7. Apply thermostat.
8. Measure properties.
9. Go to 1.

Here, \vec{x}_i is the position of atom i , \vec{v}_i and \vec{a}_i are the velocity and acceleration. Each step is understood to be performed for all atoms i . Since the updates are performed synchronously, the update for different atoms can easily be performed in parallel. In step 3. and 6., we have indicated that in case of constraints in the system, i.e., when certain distances or angles between atoms are kept constant, this should be performed at that place.

2. Constant Temperature Simulations

The most direct way to control the temperature of a system, i.e., to sample the canonical ensemble, are thermostats, applied in step 7.. For an overview on different thermostating strategies, see Ref. [43] and references therein. We implement the Berendsen, Andersen, and Lowe-Andersen thermostat [44]. These thermostats work by either rescaling the atoms velocities or by picking new velocities from the Maxwell-Boltzmann distribution for a fraction of atoms or pairs of atoms [44].

It is also possible to define equations that deviate from Newton’s equation of motion, leading for example to the Langevin and Brownian dynamics equation [43]. These integrators require adapted integration schemes [45].

Another way to control the temperature to introduce additional degrees of freedom that act as coupling to an external heatbath. This modifies the integration, where the additional degree of freedoms are explicitly integrated. We implement the Nosé–Hoover and Nosé–Hoover chain dynamics [43], which introduce one or more additional harmonic ‘particles’ that couple the system’s temperature to the target temperature.

Practically, in DIMOS, one defines all different type of thermostats or ways to perform the dynamics as separate integrators. Below, the code necessary to define the Langevin and Nosé–Hoover chain dynamics, as well as dynamics using the velocity Verlet integrator in conjunction with the Andersen thermostat is demonstrated.

```
integrator = dimos.LangevinDynamics(dt, T, gamma,
system)
integrator = dimos.NoseHooverChainDynamics(dt, T,
freq, system)
integrator = dimos.AndersenDynamics(dt, T, freq,
system)
```

3. Constant Temperature and Pressure Simulations

Finally, to reproduce many experimental conditions correctly, it is necessary to simulate the system at constant pressure. We implement an isotropic and anisotropic Monte Carlo barostat [46], which works by proposing new box sizes and accepting the new state with the usual Metropolis Monte Carlo criterion. In particular, one proposes new box sizes for the simulation cell, and then repositions the coordinates of the atoms within this box to correspond to the changed dimensions. A high acceptance rate is achieved by displacing the center of each molecule instead of treating each atom individually, as this way one avoids distortions within each molecule. Alternatively, in cases where molecules are not as clearly defined such as for MLIPs, it is also possible to simply displace every atom independently.

Following OpenMM [26], we have also implemented an option that adapts the proposal distribution heuristically so that the target acceptance rate lays within the user specified bounds. This avoids situations where either only small changes to the volume is proposed, which are then accepted very often, but lead only to small actual changes and situations where the proposed change is large, but seldom accepted due to the high energy barrier.

In DIMOS, the desired barostat is defined, and then passed together with the `system` and `integrator` to initialize the simulation object.

```
barostat = dimos.MCBarostatIsotropic(box,
target_pressure, freq)
simulation = dimos.MDSimulation(system, integrator,
positions, barostat, T)
```

4. Constraints

To enable a larger time step Δt in integration, it is common [47] to restrict the highest-frequency motions of the system, and hence to fix the involved relative positions of the atoms to their equilibrium value. This effectively allows increasing Δt such that the second-fastest motion is sampled with enough intermediate observations between oscillations.

We implement two constraint algorithms, SETTLE [21] and the constant constraint matrix approximation (CCMA) approach [22]. The former method constrains both positions and velocities by finding analytical expression for three body systems with three constraints, typical for parameterization of water molecules, such as TIP3P [14]. CCMA, on the other hand, is an iterative method that is more generally applicable for arbitrary constraint topologies. It is an iterative Lagrange multiplier-based method, in which the (inverse) of the Jacobian matrix is approximated to be constant by utilizing equilibrium expected behavior. To use constraint algorithms, DIMOS provides a keyword based option for the most common type of constraints when generating the `system`, i.e., either constraining all bonded interactions containing at least one hydrogen or additionally constraining all angles where at least one of the atoms is a hydrogen.

```
system = dimos.AmberForceField(filename,
    constraint_option="h_bonds"|"h_angles")
```

If any of the options is activated, water molecules are always constrained, following the convention of OpenMM. Whether to use SETTLE or CCMA for the list of constrained atoms is automatically determined, and does not need to be specified by the user.

If a more fine-grained control is desired, it is possible to explicitly set the `constraint_handler` object of the `integrator`:

```
integrator.constraint_handler = dimos.
    ConstraintHandling(
        constraints, constr_eq_val,
        masses, num_atoms, angle_list,
        angle_parameters, tolerance)
```

5. Energy minimization

We implement energy minimization by utilizing the optimizer framework available in `torch.optim`, usually employed for learning network parameters via back-propagation. This allows for easy access to methods like gradient descent or variants thereof including momentum terms, such as commonly used in ML. A maybe more common method for geometry optimization of molecules, also used in OpenMM [26] as standard energy minimizer, is limited-memory BFGS [48]. This is also set as standard in DIMOS.

Having already defined a simulation object, the energy can be minimized very simply by calling

```
simulation.minimize_energy(steps, optimizer="LBFGS")
# If a custom optimizer is chosen:
def optimizer(parameters): return torch.optim.Adam(
    parameters, lr=lr)
simulation.minimize_energy(steps, optimizer=optimizer)
```

This allows also the testing of some advanced optimizers developed in the ML literature to be evaluated on molecular systems.

F. Self-tuning Hamiltonian Monte Carlo Simulations

HMC [13] generates MCMC proposals by simulating (discretized) Hamiltonian dynamics. To obtain a new proposal, velocities v are first sampled from the Maxwell-Boltzmann distribution, defining the total energy $E(\mathbf{x}, \mathbf{v}) = U(\mathbf{x}) + T(\mathbf{v})$, where $U(\mathbf{x})$ is the potential energy (dependent only on positions \mathbf{x}) and $T(\mathbf{v})$ is the kinetic energy (dependent only on velocities \mathbf{v}). In practice, the system is then evolved using a volume-preserving, time-reversible integrator, such as the velocity Verlet integrator. Because phase-space volume is conserved by the integrator, the Metropolis-Hastings acceptance criterion does not require computing the Jacobian determinant.

Short trajectories of only a few integration steps L result in diffusive behavior dominated by random velocity resampling. In contrast, long trajectories in addition to adding additional computational effort risk accumulating numerical errors and redundant exploration (e.g., states “looping back”). Similarly, the integrator timestep Δt involves a trade-off: Very small Δt lead to inefficient exploration, while large Δt introduces effects from a shadow Hamiltonian or even lead to catastrophic instabilities. As shown in prior work [7], naively targeting a fixed acceptance rate (a common heuristic in the field) can fail to optimize the autocorrelation time. This is because acceptance rates only reflect energy conservation errors, not exploration quality.

Instead of tuning the acceptance rate, we optimize HMC simulation parameters via end-to-end training, using a physics-informed objective. In MCMC, a standard optimization metric is the expected squared jump distance (ESJD) [49] of a system property θ , defined as

$$\mathcal{L} = \langle (\theta' - \theta)^2 \rangle \approx \frac{1}{R} \sum_{i=0}^{R-1} \alpha_i (\theta'_i - \theta_i)^2, \quad (15)$$

where the acceptance probability

$$\alpha_i = \min(1, \exp(-(E(\mathbf{x}, \mathbf{v}) - E(\mathbf{x}', \mathbf{v}'))/k_b T)) \quad (16)$$

depends on the difference of the total energy E . Here, k_b is the Boltzmann factor, T is the temperature, \mathbf{x}, \mathbf{v} are

the starting position and (randomly picked) velocity, and \mathbf{x}', \mathbf{v}' are the proposed state. The average is computed over R independent replicas. For the application in this paper, we choose to optimize directly the movement in real space, i.e., we use $\theta = x$ and set $R = 10$.

To optimize Δt and L , we model them as folded normal variables $\mathcal{N}_F(x; \mu, \sigma)$, similar as in Ref. [50], defined on \mathbb{R}^+ with density:

$$\mathcal{N}_F(x; \mu, \sigma) = \frac{1}{\sqrt{2\pi\sigma^2}} e^{-\frac{(x-\mu)^2}{2\sigma^2}} + \frac{1}{\sqrt{2\pi\sigma^2}} e^{-\frac{(x+\mu)^2}{2\sigma^2}}. \quad (17)$$

Here, μ is learned via backpropagation [50, 51], while σ is fixed to $\sigma = 0.01\Delta t$ for Δt and $\sigma = 1$ for L . In both cases having $\sigma > 0$ functions as a way of jittering, used to avoid effects related to suboptimal performance due to the travelled distance being always the same [7]. For L , which is inherently discrete, we reweight contributions to the loss by the step count L_j , yielding:

$$\mathcal{L} = \frac{1}{R} \sum_{i=0}^{R-1} \sum_j \frac{w_j \alpha_{i,j}}{L_j} (\theta'_{i,j} - \theta_{i,j})^2 \quad (18)$$

where $w_j = \mathcal{N}_F(L_j; \mu, \sigma)$, and j indexes trajectories up to L_j . The sum is truncated at L , chosen as the quantile function of \mathcal{N}_F evaluated at 0.999. This prioritizes computational efficiency (loss per force evaluation) while avoiding infinite sums. Note that as final proposal we consider the configuration obtained after ℓ steps, where ℓ is sampled categorically from the discretized distribution of $\mathcal{N}_F(\mu, \sigma)$.

We further optimize atomic masses (cf. Fig. 3(d) and (e)): Protein masses are tuned individually, while water oxygen and hydrogen masses are shared across the water molecules. This prevents overfitting to changing solvent configurations. Optimizing the masses is possible in HMC because the partition functions for positions and velocities factorize, hence, the positional distribution is

still sampled correctly even though the dynamics does not follow a physical evolution any longer. Since changes in the *total* mass of the system is trivially equivalent to changes of Δt , we fix it to be constant and only redistributed masses among the atoms.

To assess the speed-up, we measure the autocorrelation time from the time series of the potential energy defined as

$$A(k) = \frac{\langle \mathcal{O}_t \mathcal{O}_{t+k} \rangle - \langle \mathcal{O}_t \rangle^2}{\langle \mathcal{O}_t^2 \rangle - \langle \mathcal{O}_t \rangle^2}, \quad (19)$$

where $\langle \dots \rangle$ symbolizes the thermodynamics expectation and k is the lag-time. For large k , $A(k)$ decays exponentially

$$A(k) \xrightarrow{k \rightarrow \infty} e^{-k/\tau_{\text{exp}}}, \quad (20)$$

defining the exponential autocorrelation time τ_{exp} , indicating the number of simulation steps needed to obtain uncorrelated samples.

In DIMOS, an MCMC simulation is initialized by defining specific proposal moves, which are then together with the system used to initialize simulation object:

```
hmc_move = dimos.monte_carlo.HMC(T, dt, system)
simulation = dimos.MCSimulation(system, positions, [
    hmc_move], [1.0], T)
```

It is possible to associate several types of MCMC move sets to generate a simulation object, where the different moves are picked with the probabilities specified in the associated list.

ACKNOWLEDGMENTS

We thank Fabio Müller, Falk Selker, Nicolas Weber, and Mathias Niepert for useful discussions.

-
- [1] S. A. Hollingsworth and R. O. Dror, Molecular dynamics simulation for all, *Neuron* **99**, 1129 (2018).
 - [2] W. Janke, *Rugged free energy landscapes: Common computational approaches to spin glasses, structural glasses and biological macromolecules*, Vol. 736 (Springer, Heidelberg, 2007).
 - [3] P. Friederich, F. Häse, J. Proppe, and A. Aspuru-Guzik, Machine-learned potentials for next-generation matter simulations, *Nat. Mater.* **20**, 750 (2021).
 - [4] For example, LAMMPS [38] and OpenMM [26] only recently introduced approaches to facilitate the use of MLIPs in simulations.
 - [5] A. Paszke, S. Gross, F. Massa, A. Lerer, J. Bradbury, G. Chanan, T. Killeen, Z. Lin, N. Gimelshein, L. Antiga, *et al.*, Pytorch: An imperative style, high-performance deep learning library, *Adv. Neur. Inf. Proc. Sys. (NeurIPS)* (2019).
 - [6] C. P. Goodrich, E. M. King, S. S. Schoenholz, E. D. Cubuk, and M. P. Brenner, Designing self-assembling kinetics with differentiable statistical physics models, *Proc. Nat. Acad. Sci.* **118**, e2024083118 (2021).
 - [7] H. Christiansen, F. Errica, and F. Alesiani, Self-tuning Hamiltonian Monte Carlo for accelerated sampling, *J. Chem. Phys.* **159** (2023).
 - [8] S. Doerr, M. Majewski, A. Pérez, A. Kramer, C. Clementi, F. Noe, T. Giorgino, and G. De Fabritiis, TorchMD: A deep learning framework for molecular simulations, *J. Chem. Theory Comput.* **17**, 2355 (2021).
 - [9] S. S. Schoenholz and E. D. Cubuk, JAX M.D. a framework for differentiable physics, *Adv. Neur. Inf. Proc. Sys. (NeurIPS)* (2020).
 - [10] For example, see <https://github.com/openmm/NNPOps> for implementations of neighborlists and particle-mesh Ewald methods.

- [11] M. R. Shirts, C. Klein, J. M. Swails, J. Yin, M. K. Gilson, D. L. Mobley, D. A. Case, and E. D. Zhong, Lessons learned from comparing molecular dynamics engines on the SAMPL5 dataset, *J. Comput.-Aided Mol. Des.* **31**, 147 (2017).
- [12] S. Duane, A. D. Kennedy, B. J. Pendleton, and D. Roweth, Hybrid monte carlo, *Phys. Lett. B* **195**, 216 (1987).
- [13] S. Brooks, A. Gelman, G. Jones, and X.-L. Meng, eds., *Handbook of Markov Chain Monte Carlo* (Chapman and Hall/CRC, New York, 2011).
- [14] W. L. Jorgensen, J. Chandrasekhar, J. D. Madura, R. W. Impey, and M. L. Klein, Comparison of simple potential functions for simulating liquid water, *J. Chem. Phys.* **79**, 926 (1983).
- [15] U. Essmann, L. Perera, M. L. Berkowitz, T. Darden, H. Lee, and L. G. Pedersen, A smooth particle mesh Ewald method, *J. Chem. Phys.* **103**, 8577 (1995).
- [16] A. Y. Toukmaji and J. A. Board Jr, Ewald summation techniques in perspective: A survey, *Comput. Phys. Comm.* **95**, 73 (1996).
- [17] I. Batatia, D. P. Kovacs, G. N. C. Simm, C. Ortner, and G. Csanyi, MACE: Higher order equivariant message passing neural networks for fast and accurate force fields, *Adv. Neur. Inf. Proc. Sys.* (2022).
- [18] I. Batatia, P. Benner, Y. Chiang, A. M. Elena, D. P. Kovács, J. Riebesell, X. R. Advincula, M. Asta, W. J. Baldwin, N. Bernstein, *et al.*, A foundation model for atomistic materials chemistry, arXiv:2401.00096 (2023).
- [19] A. H. Larsen, J. J. Mortensen, J. Blomqvist, I. E. Castelli, R. Christensen, M. Dułak, J. Friis, M. N. Groves, B. Hammer, C. Hargus, *et al.*, The atomic simulation environment—a Python library for working with atoms, *J. Phys. Condens. Matter* **29**, 273002 (2017).
- [20] See <https://ambermd.org/GPUPerformance.php>.
- [21] S. Miyamoto and P. A. Kollman, Settle: An analytical version of the SHAKE and RATTLE algorithm for rigid water models, *J. Comput. Chem.* **13**, 952 (1992).
- [22] P. Eastman and V. S. Pande, Constant constraint matrix approximation: a robust, parallelizable constraint method for molecular simulations, *J. Chem. Theory Comput.* **6**, 434 (2010).
- [23] P. K. Weiner and P. A. Kollman, AMBER: Assisted model building with energy refinement. A general program for modeling molecules and their interactions, *J. Comput. Chem.* **2**, 287 (1981).
- [24] C. W. Hopkins, S. Le Grand, R. C. Walker, and A. E. Roitberg, Long-time-step molecular dynamics through hydrogen mass repartitioning, *J. Chem. Theory Comput.* **11**, 1864 (2015).
- [25] A. Duval, S. V. Mathis, C. K. Joshi, V. Schmidt, S. Miret, F. D. Malliaros, T. Cohen, P. Lio, Y. Bengio, and M. Bronstein, A hitchhiker’s guide to geometric GNNs for 3D atomic systems, arXiv:2312.07511 (2023).
- [26] P. Eastman, R. Galvelis, R. P. Peláez, C. R. Abreu, S. E. Farr, E. Gallicchio, A. Gorenko, M. M. Henry, F. Hu, J. Huang, *et al.*, OpenMM 8: Molecular dynamics simulation with machine learning potentials, *J. Phys. Chem. B* **128**, 109 (2023).
- [27] B. R. Brooks, R. E. Bruccoleri, B. D. Olafson, D. J. States, S. a. Swaminathan, and M. Karplus, CHARMM: a program for macromolecular energy, minimization, and dynamics calculations, *J. Comput. Chem.* **4**, 187 (1983).
- [28] J. Kolafa and J. W. Perram, Cutoff errors in the Ewald summation formulae for point charge systems, *Molec. Sim.* **9**, 351 (1992).
- [29] L. Verlet, Computer "experiments" on classical fluids. I. Thermodynamical properties of Lennard-Jones molecules, *Phys. Rev.* **159**, 98 (1967).
- [30] M. P. Allen and D. J. Tildesley, *Computer Simulation of Liquids* (Oxford University Press, Oxford, 2017).
- [31] M. R. Shirts, D. L. Mobley, J. D. Chodera, and V. S. Pande, Accurate and efficient corrections for missing dispersion interactions in molecular simulations, *J. Phys. Chem. B* **111**, 13052 (2007).
- [32] I. G. Tironi, R. Sperb, P. E. Smith, and W. F. van Gunsteren, A generalized reaction field method for molecular dynamics simulations, *J. Chem. Phys.* **102**, 5451 (1995).
- [33] R. H. Bartels, J. C. Beatty, and B. A. Barsky, *An introduction to splines for use in computer graphics and geometric modeling* (Morgan Kaufmann, 1995).
- [34] K. Schütt, P.-J. Kindermans, H. E. Sauceda Felix, S. Chmiela, A. Tkatchenko, and K.-R. Müller, Schnet: A continuous-filter convolutional neural network for modeling quantum interactions, *Adv. Neur. Inf. Proc. Sys. (NeurIPS)* **30** (2017).
- [35] M. Neumann, J. Gin, B. Rhodes, S. Bennett, Z. Li, H. Choubisa, A. Hussey, and J. Godwin, Orb: A fast, scalable neural network potential (2024).
- [36] V. Zaverkin, F. Alesiani, T. Maruyama, F. Errica, H. Christiansen, M. Takamoto, N. Weber, and M. Niepert, Higher-rank irreducible cartesian tensors for equivariant message passing, *Adv. Neur. Inf. Proc. Sys. (NeurIPS)* (2024).
- [37] T. W. Ko and S. P. Ong, Recent advances and outstanding challenges for machine learning interatomic potentials, *Nat. Comput. Sci.* **3**, 998 (2023).
- [38] A. P. Thompson, H. M. Aktulga, R. Berger, D. S. Bolintineanu, W. M. Brown, P. S. Crozier, P. J. in ’t Veld, A. Kohlmeyer, S. G. Moore, T. D. Nguyen, *et al.*, LAMMPS - a flexible simulation tool for particle-based materials modeling at the atomic, meso, and continuum scales, *Comp. Phys. Comm.* **271**, 108171 (2022).
- [39] See <https://github.com/NVIDIA/cuEquivariance> for more details.
- [40] H. Lin and D. G. Truhlar, QM/MM: what have we learned, where are we, and where do we go from here?, *Theor. Chem. Acc.* **117**, 185 (2007).
- [41] R. Galvelis, A. Varela-Rial, S. Doerr, R. Fino, P. Eastman, T. E. Markland, J. D. Chodera, and G. De Fabritiis, NNP/MM: accelerating molecular dynamics simulations with machine learning potentials and molecular mechanics, *J. Chem. Inf. Model.* **63**, 5701 (2023).
- [42] W. C. Swope, H. C. Andersen, P. H. Berens, and K. R. Wilson, A computer simulation method for the calculation of equilibrium constants for the formation of physical clusters of molecules: Application to small water clusters, *J. Chem. Phys.* **76**, 637 (1982).
- [43] P. H. Hünenberger, Thermostat algorithms for molecular dynamics simulations, in *Advanced Computer Simulation: Approaches for Soft Matter Sciences I*, edited by C. Holm and K. Kremer (Springer Berlin Heidelberg, Berlin, Heidelberg, 2005) pp. 105–149.
- [44] E. Koopman and C. Lowe, Advantages of a Lowe-Andersen thermostat in molecular dynamics simulations, *J. Chem. Phys.* **124** (2006).
- [45] Z. Zhang, X. Liu, K. Yan, M. E. Tuckerman, and J. Liu, Unified efficient thermostat scheme for the canonical

- ensemble with holonomic or isokinetic constraints via molecular dynamics, *J. Phys. Chem. A* **123**, 6056 (2019).
- [46] J. Åqvist, P. Wennerström, M. Nervall, S. Bjelic, and B. O. Brandsdal, Molecular dynamics simulations of water and biomolecules with a Monte Carlo constant pressure algorithm, *Chem. Phys. Lett.* **384**, 288 (2004).
- [47] A. Perez, J. L. MacCallum, E. A. Coutsias, and K. A. Dill, Constraint methods that accelerate free-energy simulations of biomolecules, *J. Chem. Phys.* **143** (2015).
- [48] D. C. Liu and J. Nocedal, On the limited memory BFGS method for large scale optimization, *Math. Program.* **45**, 503 (1989).
- [49] C. Pasarica and A. Gelman, Adaptively scaling the metropolis algorithm using expected squared jumped distance, *Statistica Sinica* , 343 (2010).
- [50] F. Errica, H. Christiansen, V. Zaverkin, T. Maruyama, M. Niepert, and F. Alesiani, Adaptive message passing: A general framework to mitigate oversmoothing, oversquashing, and underreaching, arXiv:2312.16560 (2023).
- [51] F. Errica, H. Christiansen, V. Zaverkin, M. Niepert, and F. Alesiani, Adaptive width neural networks, arXiv:2501.15889 (2025).